Jurnal Kejuruteraan 36(1) 2024: 273-285
https://doi.org/10.17576/jkukm-2024-36(1)-25

Design of Fuzzy Logic based Adaptive Active Power Controller to Enhance Power sharing among DGs in an Autonomous Microgrid

Kinnari Matharani* & Hitesh Jariwala

Department of Electrical Engineering, Sardar Vallabhbhai National Institute of Technology (SVNIT), Surat, India

**Corresponding author: kinbaheti@gmail.com*

Received 6 June 2023, Received in revised form 25 July 2023
Accepted 25 August 2023, Available online 30 January 2024

ABSTRACT

This paper presents the design of an adaptive active power controller to enhance the power-sharing capabilities of distributed generators (DGs) in an autonomous microgrid. Each DG in an autonomous microgrid consists of a droop-controlled inverter to control active and reactive power by regulating frequency and voltage correspondingly. The high droop gain can be used in the power controller to encourage faster power sharing among the DGs. However, high droop gain can cause undamped growing oscillations during load fluctuations or generation losses. During such events, attaining faster power-sharing between DGs using high droop gains is difficult. So, the problem with an autonomous microgrid is the conflict between faster power sharing and stability. Stability needs to be compromised to attain quicker power sharing and vice versa. Hence, to achieve power-sharing swiftly with high droop gain and to diminish the growing oscillations caused, this paper proposes a fuzzy logic-based adaptive active power controller (FLAPC). The proposed FLAPC is adaptive and easy to implement. It offers faster power sharing for different values of droop gains and step change in load. The FLAPC is developed in MATLAB 2018a/Simulink environment, and time domain simulations are performed to see the efficacy of the proposed controller. The results of time domain simulations are compared with a droop controller without any additional controller, conventional lead-lag power system stabilizer, and proposed controller for step change in load at different droop gains. The results show that the proposed controller enhances the power-sharing performance and also ameliorates the system's stability by reducing the settling time and overshoot in active power responses of DGs.

Keywords: Power-sharing; stability; autonomous microgrid; power system stabilizer; fuzzy logic

INTRODUCTION

The traditional power generation system is undergoing profound changes due to increasing concerns about its environmental impact and the fossil energy crisis. Renewable energy generation is gaining popularity due to zero carbon emissions and fuel-free generation. Distributed generation units (DG) based on renewable energy sources such as photovoltaic systems (PV), wind energy systems (WES), and microturbines (MT) are cost-effective and environmentally friendly(Abutaima and Mohamed 2022, Harun and Kejuruter 2022, Shahgholian 2021). The integration of DGs energy storage units and different kinds of loads has emerged as the concept of a microgrid.

The key feature of the microgrid is that it can function both in grid-tied mode and autonomous mode. The operation of the microgrid in autonomous mode is crucial for stability because the system's voltage and frequency must be preserved within limits by the microgrid's controller (Farrokhabadi et al. 2019, Kljajić et al. 2020). The coordinated control techniques are employed amid parallel-connected distributed generator (DG) units to aggrandize the performance of the microgrid. Microgrids are controlled hierarchically, with primary control, secondary control, and tertiary control. (Yamashita et al. 2020, Liu, Wei, and Wang 2020). A droop controller is a decentralized form of primary control. It mimics the governor action of a traditional AC generator. In the droop controller, the reference frequency and voltage are generated depending on the average value of measured real power and reactive power. The active power-frequency droop and reactive power-bus voltage droop are employed

to maintain the frequency and bus voltages in the microgrid(Zafari et al. 2020).

The DGs in a microgrid are interconnected through power electronics converters. Therefore, they have less inertia, which makes them sensitive to changes in controller parameters, load parameters, and network parameters(Mahdavian, Ghadimi, and Bayat 2021, Shuai et al. 2018). A comprehensive microgrid model with a load model and a network model is presented in the (Pogaku, Prodanovic, and Green 2007, Raju and Jain 2019, Rasheduzzaman, Mueller, and Kimball 2014, Matharani and Jariwala 2023). It shows that the low-frequency prominent modes appearing in the system are due to droop controller parameters mainly. Therefore, the droop controller plays vital role to preserve the microgrid's stability. The high value of droop gain enhances power-sharing, but it compromises the stability of the system. Various modifications to the droop controller are suggested in the literature to improve the stability of the microgrid (Aderibole, Zeineldin, and Al Hosani 2018, Khaledian and Golkar 2017, Firdaus and Mishra 2019, Chen et al. 2016, Ebrahim et al. 2022, Li et al. 2020, Huang and Chen 2020, Kulkarni and Gaonkar 2021, Praiselin, Edward, and Technology 2022).

The analytical analysis of the effect of droop coefficients on real power and reactive power with various types of loads is presented in (Khaledian and Golkar 2017). In (Huang and Chen 2020) improved droop control approach for reactive power sharing is developed. A different configuration of a power system stabilizer (PSS)-based controller is presented in (Aderibole, Zeineldin, and Al Hosani 2018, Firdaus and Mishra 2019, Jia et al. 2020). In (Aderibole, Zeineldin, and Al Hosani 2018), the stability of a multi-microgrid consisting of an inverter-coupled and synchronous generating unit is assessed by placing PSS using residue analysis. Conventional single-stage PSS (CPSS) was developed (Firdaus and Mishra 2019) to improve the power-sharing and stability of a four-inverter autonomous microgrid. In (Jia et al. 2020) multi-stage lead-lag compensator-based droop controller is designed. The adaptive virtual impedance droop control is suggested in (Li et al. 2020) for different source output and load demands.

The power-sharing is enhanced in (Kulkarni and Gaonkar 2021) by introducing additional terms in droop equations based on the impedance of the distribution line. Power differential droop gain is proposed by (Chen et al. 2016) to enhance the power-sharing of a grid-connected microgrid. But it is difficult to select the proper value of differential droop gains. Arctan function-based virtual impedance control is developed in (Gajbhiye and Khatri 2021). Conventional droop control, in combination with a derivative and integral controller, is used to enhance power loop dynamics in islanded and grid-tied modes (Kim et al. 2010).

The inverter control parameters are optimized using different optimization techniques in (Yu et al. 2015, Ebrahim et al. 2022, Shi et al. 2022, Zhang et al. 2019). Multivariable angle droop control for quicker power-sharing in PV and WES is developed in (Praiselin, Edward, and Technology 2022). Power-sharing in stand-alone microgrid with angle droop control is proposed (Kolluri et al. 2017, John, Ghosh, and Zare 2017). Optimal angle droop control with a flatness controller is developed in (Moussa et al. 2017). But frequency droop provides better power-sharing as compared to angle droop control. It is challenging to determine the value of the tuning parameters in all of the droop controllers previously proposed. The fuzzy logic-based active power controller (FLAPC) developed in this paper is adaptive and improves active power-sharing for low and high values of real power droop gain. The power-sharing is prosecuted faster, and the transient response is improved with the proposed FLAPC.

THE MAIN CONTRIBUTIONS OF THIS PAPER ARE:

1. The comprehensive mathematical model of the droop-controlled inverter coupled DG-based microgrid is developed.
2. The FLAPC is developed considering a triangular membership function and 49 rules which is adaptable and does not require any tuning parameters like other controllers.
3. The efficaciousness of the developed novel FLAPC is compared with CPSS and typical droop controllers without any additional controller.

The remnant paper is condensed as follows. Section 2 provides information regarding the system being studied and its control approach. Section 3 illustrates the issue of inadequate dampening by demonstrating the effect of the droop coefficient on microgrid stability. Following a design procedure of the proposed Fuzzy logic-based active power controller in Section 4, Section 5 shows the outcome of the simulation results. Finally, this paper is concluded in Section 6.

MATHEMATICAL MODEL OF THE STUDY SYSTEM

The system under study is displayed in Figure 1. It consists of three parallel-connected inverter-interfaced DGs. The DGs are outfitted with droop controllers to satisfy the power needs while regulating the system voltage and frequency. The droop gains of all the DGs are kept identical to share

the active power uniformly. The modeling of microgrid is divided into different submodules: Droop controlled inverter interfaced DGs, load, and network model. Each DG unit is represented by its own reference frame, the rotation frequency of which is determined by the power-sharing controller. The network and load models are formulated using a common reference frame.

The mathematical model of individual submodules is developed and integrated to extract the entire model of the microgrid. The section below provides further information on the system's mathematical modelling.

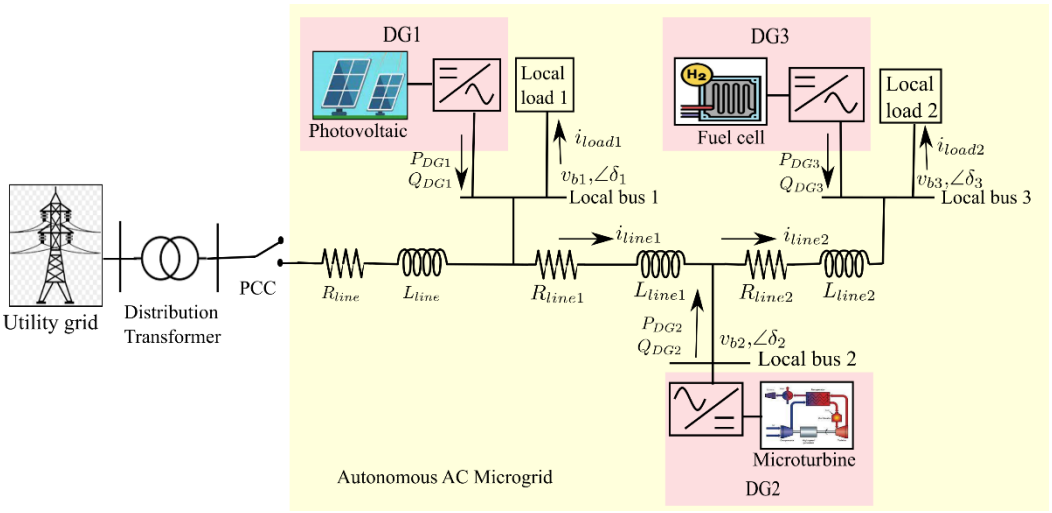

FIGURE 1. Schematic diagram of the study system

MATHEMATICAL MODEL OF DROOP-CONTROLLED INVERTER COUPLED DG

The DG units in a microgrid are interfaced with the network using three-phase voltage source inverters (VSI), LC filters, and coupling inductors, as depicted in Figure 2. The switching operation of the inverter is omitted due to the high frequency of VSI. The DC voltage obtained from renewable energy sources is assumed constant, and the dynamics of the DC side are neglected. The droop controller of VSI consists of an outer power-sharing controller, an inner voltage controller, and a current controller. The detailed model of the individual part is described below correspondingly.

POWER CONTROLLER

The power controller consists of a droop control that generates reference voltage and reference frequency for each DG. The powers (active and reactive) are shared amid all the DGs depending on generated references. The output voltages (v_{od},) and output currents (i_{od},) of the DGs in dq reference frame is utilized to obtain instantaneous real power (p_{in}) and reactive power (q_{in}) as presented in Equations (1) and (2).

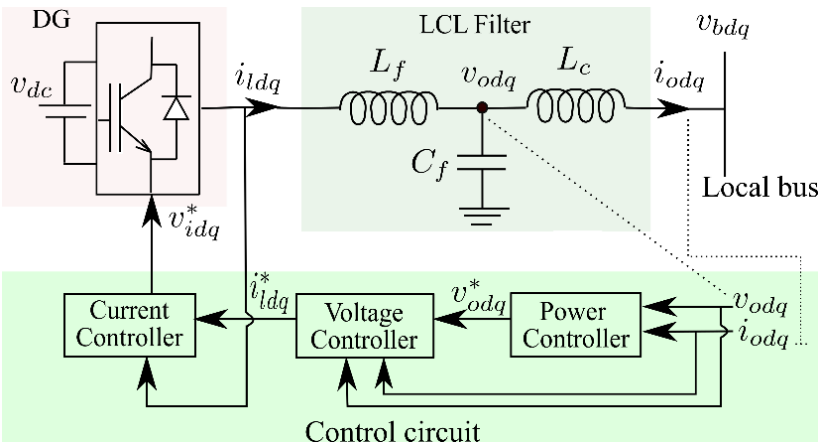

FIGURE 2. Interface circuit of DG including controllers and LCL filter

$$p_{in} = v_{od} i_{od} + v_{oq} i_{oq} \quad (1)$$

$$q_{in} = v_{oq} i_{od} - v_{od} i_{oq} \quad (2)$$

The average active and reactive power (P and Q) are derived from instantaneous power (p_{in} and q_{in}) using a low pass filter (LPF), as shown in Figure 3. The extraction of average powers is expressed as,

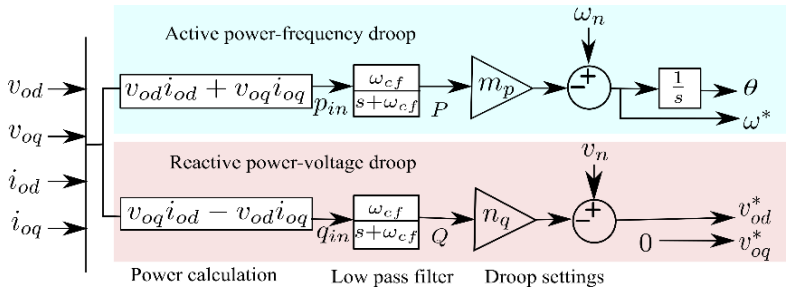

FIGURE 3. Mathematical model of power controller

$$P = \frac{\omega_{cf}}{s + \omega_{cf}} p_{in}, \dot{P} = -P\omega_{cf} + \omega_{cf} p_{in} \quad (3)$$

$$Q = \frac{\omega_{cf}}{s + \omega_c f} q_{in}, \dot{Q} = -Q\omega_{cf} + \omega_{cf} q_{in} \quad (4)$$

Where ω_{cf} is the cut-off frequency of the LPF.

The angular reference frequency (ω^*) and d-axis reference voltage (v_{od}^*) are obtained based on real power droop gain (m_p) and reactive power droop gain (n_q) from the natural frequency(ω_n) and nominal voltage $(v_{od,n})$ as shown in (5) and (6). The q-axis reference voltage is set to zero.

$$\omega^* = \omega_n - m_p P \quad (5)$$

$$v_{od}^* = v_{od,n} - n_q Q \quad (6)$$

$$v_{oq}^* = 0 \quad (7)$$

The reference transformation angle δ_j is defined for each j^{th} DG inverter to transform from an individual reference frame (dq) to a common reference frame (DQ) as,

$$\delta_j = \int (\omega_j - \omega_{com}) dt \quad (8)$$

where ω_j is the reference frequency of the j^{th} DG inverter and ω_{com} is the reference frequency of DG1 inverter, which serves as base frequency.

VOLTAGE CONTROLLER AND CURRENT CONTROLLER

The voltage controller and current controller consist of the standard proportional and integral controller. They generate reference filter inductor currents (i_{ld}^*, i_{lq}^*) and reference inverter output voltages (v_{id}^*, v_{iq}^*) respectively as represented in Figure 4. The state equations for the voltage controller are described in (7) and (8), and algebraic equations in (9) and (10).

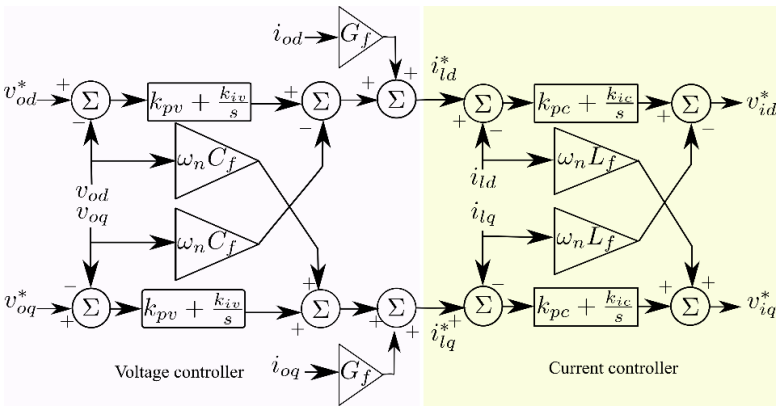

FIGURE 4. Mathematical model of voltage controller and current controller

$$\frac{d\phi_d}{dt} = v_{od}^{*} - v_{od} \quad (9)$$

$$\frac{d\phi_q}{dt} = v_{oq}^{*} - v_{oq} \quad (10)$$

where, $\emptyset_d$ and $\emptyset_q$ are state variables of the voltage controller

$$i_{ld}^{*} = G_f i_{od} - \omega_n C_f v_{oq} + k_{pv}(v_{od}^{*} - v_{od}) + k_{iv}\phi_d \quad (11)$$

$$i_{lq}^{*} = G_f i_{oq} + \omega_n C_f v_{od} + k_{pv}(v_{oq}^{*} - v_{oq}) + k_{iv}\phi_q \quad (12)$$

Where G_f is feed-forward gain, C is filter capacitance, k_{pv} and k_{iv} are proportional and integral gains of the voltage controller, correspondingly.

The state equations for the current controller are described in (11) and (12), and algebraic equations in (13) and (14).

$$\frac{d\gamma_d}{dt} = i_{ld}^{*} - i_{ld} \quad (13)$$

$$\frac{d\gamma_q}{dt} = i_{lq}^{*} - i_{lq} \quad (14)$$

where, γ_d and γ_q are state variables of current controller and i_{ld} and i_{lq} are filter inductor currents.

$$v_{id}^{*} = -\omega_n L_f i_{lq} + k_{pc}(i_{ld}^{*} - i_{ld}) + k_{ic}\gamma_d \quad (15)$$

$$v_{iq}^{*} = \omega_n L_f i_{ld} + k_{pc}(i_{lq}^{*} - i_{lq}) + k_{ic}\gamma_q \quad (16)$$

where, L_f is filter inductance, k_{pc} and k_{ic} are proportional and integral gain of current controller, respectively.

MATHEMATICAL MODEL LC FILTER AND COUPLING INDUCTOR MODEL

LC filter with coupling inductor forms an LCL filter that provides higher attenuation to harmonics and improved performance with a low value of L and C. The inverter output voltage (v_{id} and v_{iq}) is assumed to be the same as the reference output voltage (v_{id}^{*} and v_{iq}^{*}) produced by the current controller.

The state equations for LCL filter inductor currents, output currents, and output voltages are presented by,

$$\frac{di_{ld}}{dt} = \omega i_{lq} + \frac{1}{L_f}(v_{id} - v_{od} - r_f i_{ld}) \quad (17)$$

$$\frac{di_{lq}}{dt} = -\omega i_{ld} + \frac{1}{L_f}(v_{iq} - v_{oq} - r_f i_{lq}) \quad (18)$$

$$\frac{di_{od}}{dt} = \omega i_{oq} + \frac{1}{L_c}(v_{od} - v_{bd} - r_c i_{od}) \quad (19)$$

$$\frac{di_{oq}}{dt} = -\omega i_{od} + \frac{1}{L_c}(v_{oq} - v_{bq} - r_c i_{oq}) \quad (20)$$

$$\frac{dv_{od}}{dt} = \omega v_{oq} + \frac{1}{C_f}(i_{ld} - i_{od}) \quad (21)$$

$$\frac{dv_{oq}}{dt} = -\omega v_{od} + \frac{1}{C_f}(i_{lq} - i_{oq}) \quad (22)$$

where, L_c is coupling inductor, r_c and r_f are the internal resistance of the coupling inductor and filter inductor, respectively. The v_{bd} and v_{bq} are local bus voltages, and ω is the reference frequency of DG.

MATHEMATICAL MODEL OF AN INDIVIDUAL DG

The complete mathematical model of each inverter-coupled DG is formed by using (1)-(20). Each DG in a microgrid is modeled using an individual reference frame. The reference frequency of DG1 is taken as the base frequency, and all other DG variables are transformed.

The transformation technique defined in (23) is used to translate all of the other DGs from local reference (*dq*) to common reference frame (*DQ*).

$$\begin{bmatrix} f_{DQ} \end{bmatrix} = \begin{bmatrix} \cos(\delta_j) & -\sin(\delta_j) \\ \sin(\delta_j) & \cos(\delta_j) \end{bmatrix} \begin{bmatrix} f_{dq} \end{bmatrix} \quad (23)$$

The mathematical model of an individual inverter coupled DG is presented as,

$$\begin{bmatrix} \dot{\Delta x}_{DGi} \end{bmatrix} = A_{DGi}\begin{bmatrix} \Delta x_{DGi} \end{bmatrix} + B_{DGi}\begin{bmatrix} \Delta v_{bDQi} \end{bmatrix} + \ldots B_{i\omega com}\begin{bmatrix} \Delta \omega_{com} \end{bmatrix} \quad (24)$$

$$\begin{bmatrix} \Delta\omega_{DGi} \\ \Delta i_{oDGi} \end{bmatrix} = \begin{bmatrix} C_{DGi} \end{bmatrix}\begin{bmatrix} \Delta x_{DGi} \end{bmatrix} \quad (25)$$

$$\begin{bmatrix} \Delta x_{DGi} \end{bmatrix} = \begin{bmatrix} \Delta\delta_i & \Delta P_i & \Delta Q_i & \Delta\phi_{dqi} & \Delta\gamma_{dqi} & \Delta i_{ldqi} & \Delta v_{odqi} & \Delta i_{odqi} \end{bmatrix} \quad (26)$$

Where, A_{DGi} is state matrix, B_{DGi} is input matrix, C_{DGi} is output matrix and X_{DGi} is the state vector matrix of i^{th} DG.

MATHEMATICAL MODEL OF ALL INVERTER-COUPLED DGS

In a microgrid, there can be many DGs connected parallel to each other. The mathematical model of parallel connected DGs can be presented as,

$$\left[\Delta \dot{X}_{DG}\right] = A_{DG}\left[\Delta X_{DG}\right] + B_{DG}\left[\Delta v_{bDQ}\right] \quad (27)$$

$$\left[\Delta i_{oDQ}\right] = C_{DG}\left[\Delta X_{DG}\right] \quad (28)$$

$$\left[\Delta X_{DG}\right] = \left[\Delta x_{DG1} \quad \Delta x_{DG2} \quad \Delta x_{DG3} \ldots\ldots \Delta x_{DGn}\right] \quad (29)$$

Where, A_{DG} is state matrix, B_{DG} is input matrix, C_{DG} is output matrix and X_{DG} is state vector matrix of all the DGs.

NETWORK AND PASSIVE LOAD MODEL

The network, i.e., the distribution line that interconnects DGs and load, is modeled by the RL circuit (R_{linei} and L_{linei}). The state equations for line currents (i_{lineD} and i_{lineQ}) are presented as,

$$\frac{di_{lineDi}}{dt} = \frac{-R_{linei}}{L_{linei}} i_{lineDi} + \omega i_{lineQi} + \frac{1}{L_{linei}} v_{bDj} - \frac{1}{L_{linei}} v_{bDk} \quad (30)$$

$$\frac{di_{lineQi}}{dt} = \frac{-R_{linei}}{L_{linei}} i_{lineQi} - \omega i_{lineQi} + \frac{1}{L_{linei}} v_{bQj} - \frac{1}{L_{linei}} v_{bQk} \quad (31)$$

The passive load (R_{loadi} and L_{loadi}) connected at i^{th} node of the microgrid. The state equations for load currents (i_{loadD} and i_{loadQ}) are presented as,

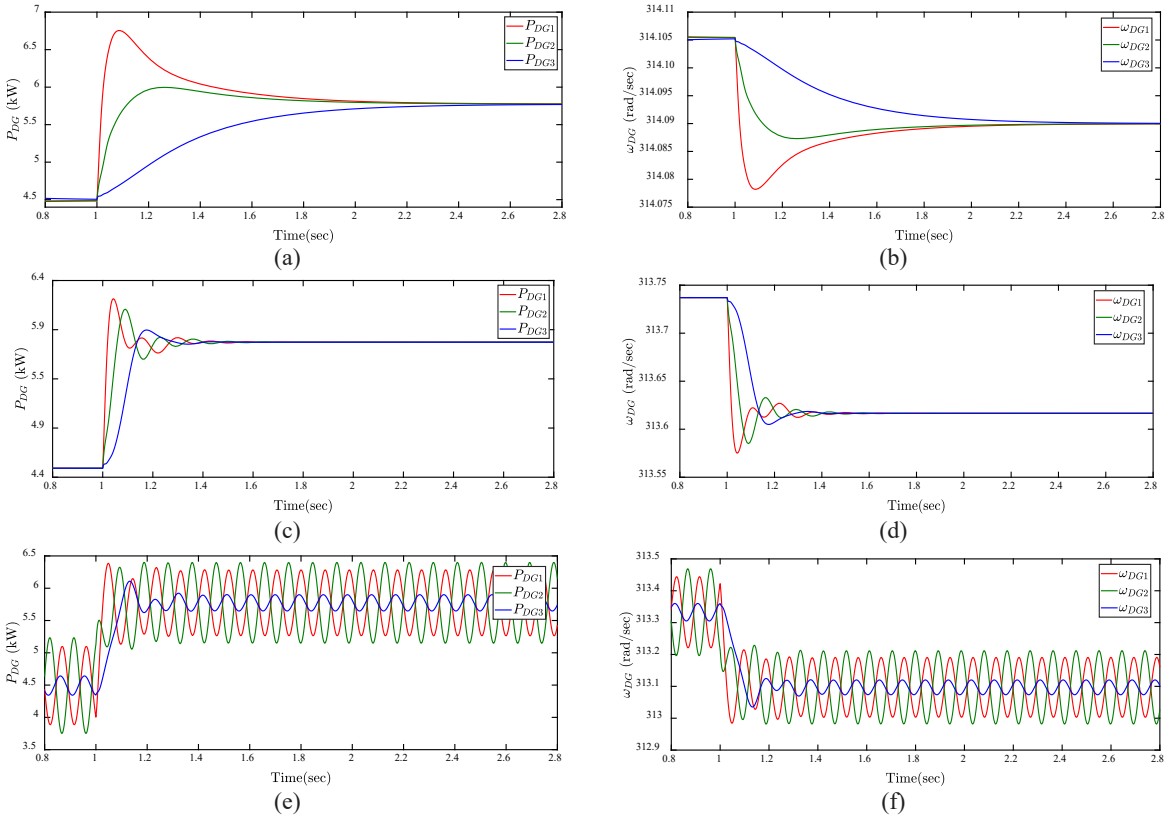

FIGURE 5. Power-sharing and frequency variation for conventional droop with different value of real power droop gain (m_p) (a) active power variation with $m_p = 1.2 \times 10^{-5}$, (b) frequency variation with $m_p = 1.2 \times 10^{-5}$, (c) active power variation with $m_p = 9.4 \times 10^{-5}$ (d) frequency variation with $m_p = 9.4 \times 10^{-5}$, (e) active power variation with $m_p = 1.84 \times 10^{-4}$ (f) frequency variation with $m_p = 1.84 \times 10^{-4}$

Figures 5(a) to 5(f) displays the simulation results of active power and frequency for different values of m_p. In Figures 5(a) and 5(b), the value of m_p is very low (1.2×10^{-5}). The equal power sharing is achieved by all the DGs in almost 1.5sec, so the difference in frequency also appears for a longer duration. The power-sharing is improved by increasing the value of m_p from 1.2×10^{-5} to 9.4×10^{-5}; because of increased $m_{p,}$ the power-sharing is improved, and load is shared equally in 0.5 sec, but oscillations appear in power and frequency responses as shown in Figures 5(c) and 5(d). Further increasing m_p (1.84×10^{-4}), the system becomes marginally stable, as displayed in Figures 5(e) and 5(f). Therefore, there is a trade-off between system stability and faster power sharing. Furthermore, larger steady-state frequency deviation is also caused by a higher droop coefficient.

$$\frac{di_{loadDi}}{dt}=\frac{-R_{loadi}}{L_{loadi}}i_{loadDi}+\omega i_{loadQi}+\frac{1}{L_{loadi}}v_{bDi} \tag{32}$$

$$\frac{di_{loadQi}}{dt}=\frac{-R_{loadi}}{L_{loadi}}i_{loadQi}-\omega i_{loadQi}+\frac{1}{L_{loadi}}v_{bQi} \tag{33}$$

COMPLETE MICROGRID MODEL

The input variables v_{bDQ} are derived by introducing a large virtual shunt resistor at each local bus node. At each node, voltage is calculated considering the incoming current as positive and the outgoing current as negative.

The node voltages at each local bus are defined as,

$$v_{bDi}=r_{VN}(i_{oDi}-i_{loadDi}+i_{lineDi,j}) \tag{34}$$

$$v_{bDi}=r_{VN}(i_{oDi}-i_{loadDi}+i_{lineDi,j}) \tag{35}$$

Where r_{VN} is virtual resistance.

The complete mathematical model of the study system is provided,

$$\begin{bmatrix}\dot{\Delta x}_{DG}\\ \Delta i_{lineDQ}\\ \Delta i_{loadDQ}\end{bmatrix}=A_{mg}\begin{bmatrix}\Delta x_{DG}\\ \Delta i_{lineDQ}\\ \Delta i_{loadDQ}\end{bmatrix} \tag{36}$$

where A_{mg} is the system state matrix.

EFFECT OF DROOP GAIN IN INVERTER-BASED MICROGRID

In a traditional power system, a parallel-operating synchronous generator consists of a governor. The increase and decrease in load demand are compensated by a decrease or increase in generation frequency. The load is shared among the different generators based on their frequency differences. The power-sharing appears across different generators until their frequency becomes equal. The real power droop equation described in Equation (5) shows the variation in the frequency with variation in load. If the value of m_p is high, the drop in frequency will be high, which causes the DG to share power instantly. But the variation in frequency due to load change is not immediate owing to the lag induced by the LPF. The change in frequency occurs after some time delay which results in oscillations in the supply frequency.

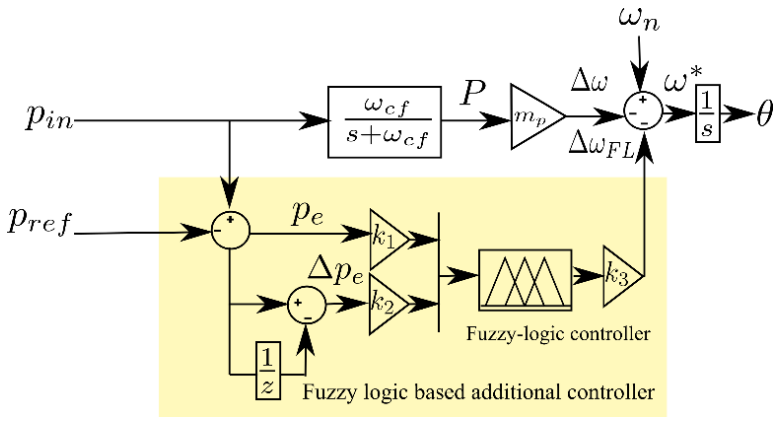

FIGURE 6. Simplified diagram of Fuzzy logic based adaptive active controller (FLAPC)

FUZZY LOGIC-BASED ADAPTIVE ACTIVE POWER CONTROLLER

Fuzzy logic is a knowledge base system for control operations. The fuzzy logic control (FLC) technique appears to be most convenient whenever a well-defined control objective is not determined. The system to be controlled is intricate, or its exact mathematical model is not available. FLC has evolved as a promising technology and is currently employed in various power system applications. (Bhukya and Mahajan 2018).

The FLC is one of the most promising techniques for converting language control rules into operational mechanisms. FLC paradigm closely resembles the intuitiveness of expert operation, making it appealing and straightforward to integrate heuristic rules in the controller that takes into account the experiences of human experts (Rahmani-Andebili 2021).

The FLC does not depend on an exact mathematical representation of the system. It accommodates parameter fluctuation effectively and can cope with disturbances. FLC modeling is simpler than conventional or model-based controllers (Gupta and Sambariya 2017).

Due to the benefits described above, the FLC-based active power controller is designed in this paper. The following section describes the design steps of FLAPC.

DESIGN PROCEDURE OF FLAPC

The FLAPC generates an additional signal $\Delta\omega_{FL}$ based on real power changes to improve the system performance. The schematic diagram of FLAPC is depicted in Figure 6.

DEFINING INPUT AND OUTPUT VARIABLES

The first stage in modeling the FLAPC is defining the system performance variables. The real power deviation (p_e) and change in real power deviation (Δp_e) are selected as input signals to the Fuzzy logic base controller. k_1 and k_2 are normalization factors and k_3 is the de-normalization factor.

MEMBERSHIP FUNCTION

In fuzzy logic systems, linguistic variables are used to express input and output variables. The number of rules increases with linguistic variables, which complicates the controller design. Different types of membership functions (MF) like Triangular, Trapezoidal. Gaussian etc. Here, seven linguistic variables with triangular MF are selected for each input and output variable, as depicted in Figure 7. The MFs of the control variables have 50% overlap between neighboring fuzzy subsets.

INFERENCE MECHANISM

The correlation between the input and output of FLC is defined by a set of rules. The rules are specified by linguistic variables using the available information in the domain of designing PSS. To achieve precise control action and make considerable difference between fuzzy regions, seven control actions named “Large Negative (LN),”

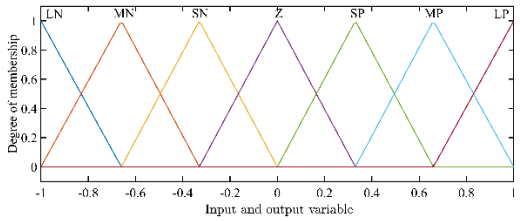

FIGURE 7. MF for input and output of 7× 7 FLC.

“Medium Negative (MN)”, “Small Negative (SN)”, “Zero (Z)”, “Large Positive (LP),” “Medium Positive (MP)”, and “Small Positive (SP)” is used(Song and Johns 1997). The LN indicates that the drop in the control variable is much larger compared to the required value, and LP means the increase in the control variable is much larger compared to the required value. The two input variables change in real power (real power error), and the change of real power error results in 49 rules for each DG, as shown in Table 1. The rules can be represented in surface view as depicted in Figure 8.

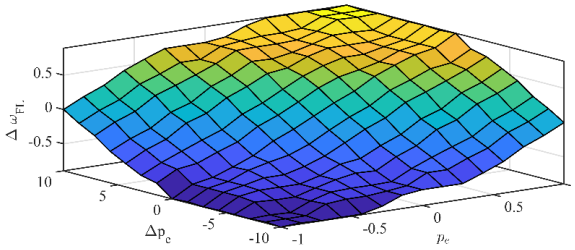

FIGURE 8. Surface view of fuzzy logic-based APC rules

THE TYPICAL STRUCTURE OF RULES IS AS FOLLOWS:

Rule 1: If the error in real power is LN and the change in real power error is LN then the frequency (output of FLC-based additional controller) is LN.

Rule 2: If the error in real power is LN and the change in real power error is MN then the frequency (output of FLC-based additional controller) is LN.

Similarly, other rules are formed, as given in Table 1 below.

TABLE 1. Rule Base

Error in real power (p_e)	change in real power error (Δp_e)						
	LN	MN	SN	Z	SP	MP	LP
LN	LN	LN	LN	LN	MN	SN	Z
MN	LN	LN	MN	MN	SN	Z	SP
SN	LN	MN	MN	SN	Z	SP	MP
Z	MN	MN	SN	Z	SP	MP	MP
SP	MN	SN	Z	SP	MP	MP	LP
MP	SN	Z	SP	MP	MP	LP	LP
LP	Z	SP	MP	LP	LP	LP	LP

SIMULATION RESULT

To assess the efficacy of the FLAPC, simulations are carried out for the different value of real power droop gain m_p. The microgrid model is implemented for sudden load shift simulation in the MATLAB/Simulink environment, and results are analyzed without PSS considering only conventional droop, with CPSS, and with developed FLAPC.

The DGs controller parameters are listed in the Appendix. The parameters of CPSS are obtained from the design procedure given by (Firdaus and Mishra 2019). The simulation sequence is: for time t=0 to t=1 sec, the system supplying the initial operating load of 25Ω load connected at node 1 and 20Ω load connected at node 3, at time t=1 sec, the step change of 3.8 kW is applied in the load at local bus 1. The simulations are performed for nominal, critical, and very high values of droop gain.

CASE 1: SIMULATION RESULTS WHEN m_p=9.4×10^{-5}

Figure 9 depicts the power delivered by different DGs with a nominal value of droop gain ($m_p = 9.4 \times 10^{-5}$). The comparison of system response is given in Table 2. The oscillations in DG1 power response are high compared to DG2 and DG3 because it is located near the load center. At a normal value of droop gain, the system is stable, but equal power sharing is achieved at 0.6 sec, and also oscillations are more in power output without any controller. The power is shared equally and without any oscillations with the proposed controller. The overshoot in real power is reduced by 0.76%, 0.69%, and 0.11%, and settling time is reduced by 0.03, 0.033, 0.17 sec with FLAPC for DG1, DG2, and DG3 as compared to CPSS, respectively. Hence with proposed controller power can be shared proportionally at lower or nominal value of droop gains by maintaining stability.

TABLE 2. Comparison of system performance with Conv. droop, with CPSS and with FLAPC for m_p = 9.4×10^{-5}

P_{DG}	Settling time (sec)			Overshoot (%)		
	Conv. droop	With CPSS	With FLAPC	Conv. droop	With CPSS	With FLAPC
P_{DG1}	0.835	0.28	0.248	7.65	2.89	2.13
P_{DG2}	0.84	0.296	0.263	5.8	1.02	0.32
P_{DG3}	0.748	0.419	0.253	2.1	0.59	0.48

CASE 2: SIMULATION RESULTS WHEN m_P=1.84×10^{-4}

Figure 10 shows the power-sharing of different DGs for the critical value of droop gain (m_p =1.84×10^{-4}). The comparison of system response is given in Table 3. The system becomes marginally stable for $m_p = 1.84 \times 10^{-4}$ with conventional droop control and oscillations in power response continues for a longer duration. The system response becomes stable, and oscillations don't appear in the power response of all DGs with CPSS and FLAPC. The overshoot in real power is reduced by 0.087%,.30%, and 0.38% and settling time is and settling time is reduced by 0.03, 0.06, 0.074 sec with FLAPC for DG1, DG2, and DG3 as compared to CPSS respectively. A considerable improvement is obtained in power sharing and settling time with FLAPC.

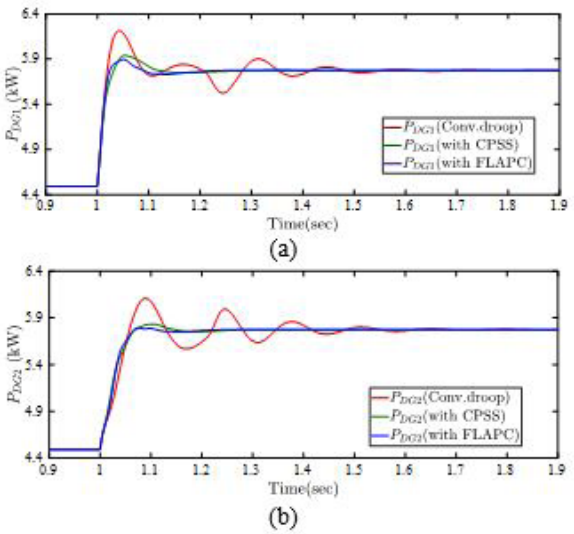

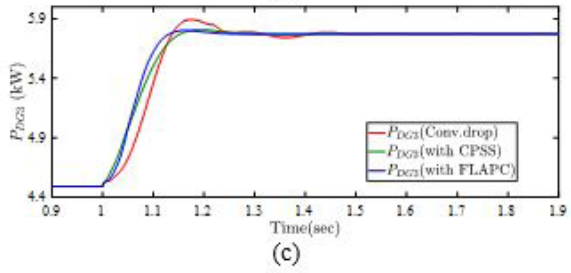

FIGURE 9. Power-sharing among different DGs for $m_p = 9.4 \times 10^{-5}$ with Conv. droop, with CPSS, and with FLAPC (a)DG1 (b) DG2(c) DG3

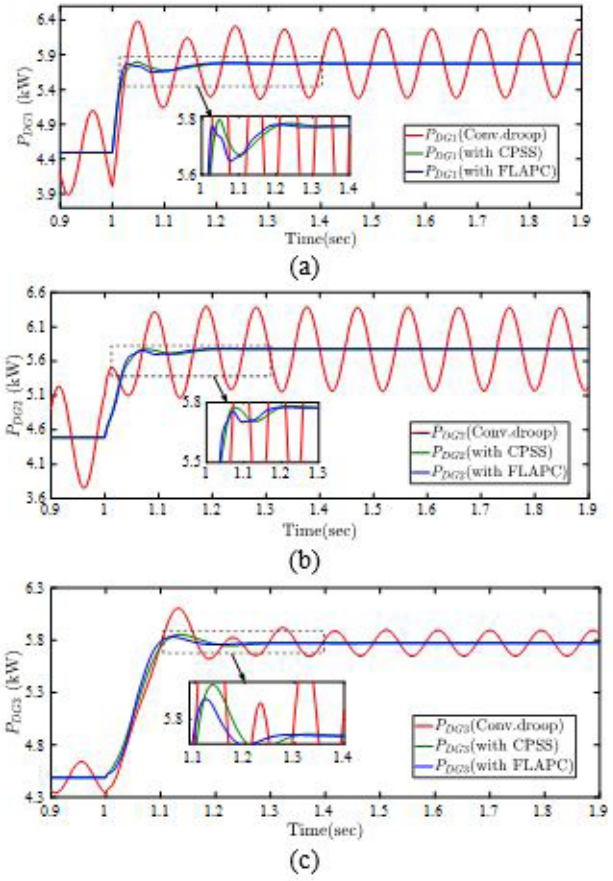

FIGURE 10. Power-sharing among different DGs for $m_p = 1.84 \times 10^{-4}$ Conv. droop, with CPSS, and with FLAPC (a) DG1 (b) DG2 (c) DG3

CASE 3: SIMULATION RESULTS WHEN m_P=2.5×10^{-4}

Figure 11 shows the power-sharing of different DGs for m_p=2.5×10^{-4} (high value). The comparison of system response is given in Table 4. The oscillations are growing and system is unstable for high value of droop gain with normal droop as shown in Figure11. At the higher value of droop gain, the power-sharing is improved with maintaining system stability in the case with CPSS and with FLAPC. The overshoot and settling time are reduced by 0.1%, 0.35%, 0.64%, and 0.107, 0.223, and 0.046 sec with FLAPC compared to CPSS for DG1, DG2, and DG3, respectively.

TABLE 3. Comparison of system performance with Conv. droop, with CPSS and with FLAPC for m_p = 1.84×10^{-4}

P_{DG}	Settling time (sec)			Overshoot (%)		
	Conv. droop	With CPSS	With FLAPC	Conv. droop	With CPSS	With FLAPC
P_{DG1}	marginally stable	0.296	0.265	-	0.14	0.052
P_{DG2}	marginally stable	0.38	0.319	-	0.42	0.12
P_{DG3}	marginally stable	0.393	0.319	-	1.42	1.04

CASE 4: SIMULATION RESULTS WHEN PSS IS SWITCHED t= 2SEC

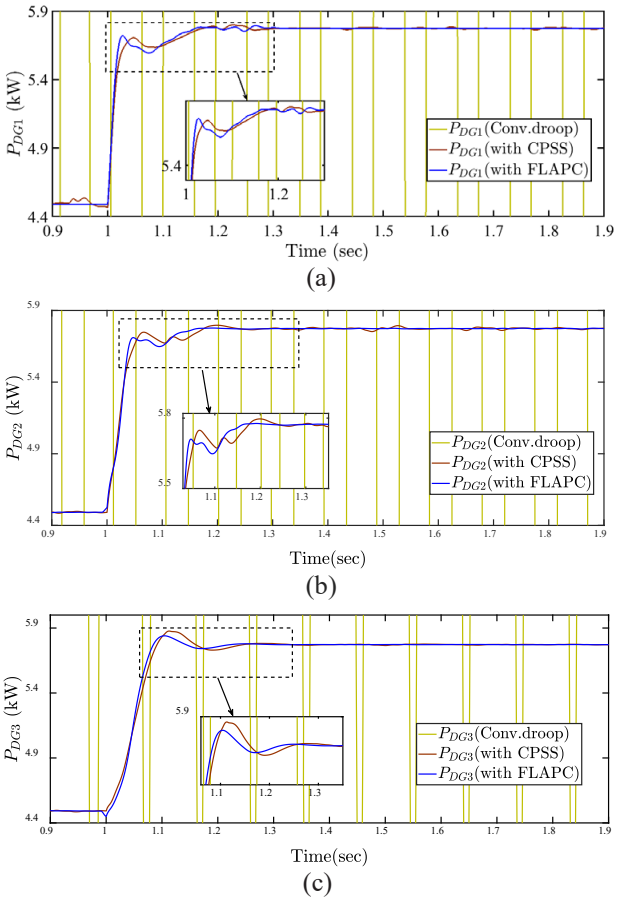

FIGURE 11. Power-sharing among different DGs for $m_p = 2.5 \times 10^{-4}$ with Conv. droop, with CPSS, and with FLAPC (a) DG1 (b) DG2 (c) DG3

Figure 12 shows the power-sharing of different DGs for $m_p = 1.9 \times 10^{-4}$. The system response is unstable, and increasing oscillations appear in the power response of all the DGs. The controller is switched on at t=2 sec. The system becomes stable in less than 0.2 sec, and overshoot is decreased considerably in the case of FLAPC as compared to CPSS.

TABLE 4 Comparison of system performance with Conv. droop, with CPSS and with FLAPC for $m_p = 2.5\times10^{-4}$

P_{DG}	Settling time (sec)			Overshoot (%)		
	Conv. droop	With CPSS	With FLAPC	Conv. droop	With CPSS	With FLAPC
P_{DG1}	unstable	0.433	0.326	-	0.45	0.35
P_{DG2}	unstable	0.53	0.307	-	0.42	0.07
P_{DG3}	unstable	0.4	0.354	-	1.80	1.16

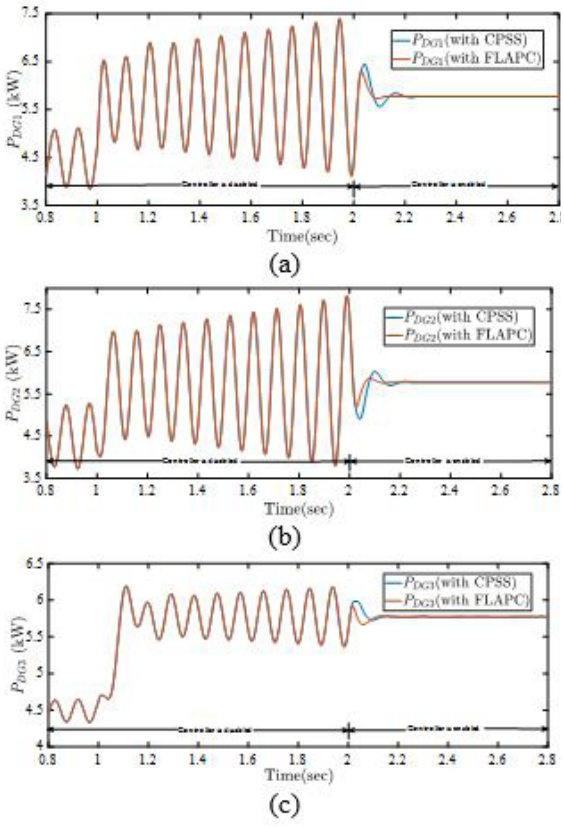

FIGURE 12. Power-sharing among different DGs for $m_p = 1.9 \times 10^{-4}$ with CPSS, and with FLAPC when controller is switched on at t=2 sec (a) DG1 (b) DG2 (c) DG3

CONCLUSION

In this paper, a design of an adaptive active power controller is proposed to enhance power-sharing among distributed generators (DGs) in an autonomous microgrid. In order to achieve fast power-sharing among the DGs to recompense the load change, the high droop gain in conventional active power controllers can cause severe oscillations. To dampen the sustained oscillations, this paper proposes an adaptive fuzzy logic-based active power control technique for an inverter coupled DG based autonomous microgrid.

The proposed FLAPC modulates the frequency according to load change by taking precise control action using the designed fuzzy rules based on the magnitude of the error. The proposed FLAPC is adaptive and avoids the tedious process of obtaining tuning parameters. The simulation results show the comparison of different active power controllers using high droop to recompense the load change. The FLAPC reduces overshoot in the range of 2% to 6%, and settling time is reduced from 0.7 sec to 0.1 sec compared to the conventional droop controller for nominal gain. The settling time and peak overshoot are also less for other values of droop gains.

During load change, the incorporation of FLPAC with DGs by enhancing the power sharing from DGs by quickly dampening the oscillations. Conclusively, the simulation results reveal that the fuzzy control technique has superior power regulation, faster oscillation dampening, and significantly reduced settling time.

ACKNOWLEDGEMENTS

The authors are grateful to Sardar Vallabhbhai National Institute of Technology for supporting this research.

DECLARATION OF COMPETING INTEREST

None

APPENDIX

Table A-1 DG controller parameters

f_s	8 kHz	m_p	9.4×10^{-5}
L_f	1.35 *mH*	n_q	1.3×10^{-3}
C_f	50 µF	k_{pv}	0.05
r_f	0.1 Ω	k_{iv}	390
L_c	0.35 mH	k_{pc}	10.5
r_{Lc}	0.03 Ω	k_{ic}	16×10^3
ω_c	31.41 rad/sec	F	0.75

Table A-2 CPSS parameters

k	9.5297×10^{-5}	T_2	0.001
T_1	0.0390	T_w	3

REFERENCES

Abutaima, Khaleel Abed, and Ramizi Jurnal Kejuruteraan Mohamed. 2022. Design of Improved Incremental Conductance with Fast Intelligent (FI) Based MPPT Technique for Solar PV System. 34 (6):1093-1104.

Aderibole, Adedayo, Hatem H Zeineldin, and Mohamed Al Hosani. 2018. A critical assessment of oscillatory modes in multi-microgrids comprising of synchronous and inverter-based distributed generation. *IEEE Transactions on Smart Grid* 10 (3): 3320-3330.

Bhukya, Jawaharlal, and Vasundhara. 2018. Fuzzy logic based control scheme for doubly fed induction generator based wind turbine. *International Journal of Emerging Electric Power Systems Mahajan* 19(6).

Chen, Xin, Changhua Zhang, Qi Huang, and Mark Ofori-Oduro. 2016. Small-signal modeling and analysis of grid-connected inverter with power differential droop control. *Mathematical Problems in Engineering* 2016.

Ebrahim, Mohamed A, Reham M Abdel Fattah, Ebtisam M Saied, Samir M Abdel Maksoud, Hisham. 2022. Salp swarm optimization with self-adaptive mechanism for optimal droop control design. *J Electric Power Conversion El Khashab, and Micro-Grids*.

Farrokhabadi, Mostafa, Claudio A Canizares, John W Simpson-Porco, Ehsan Nasr, Lingling Fan, Patricio A Mendoza-Araya, Reinaldo Tonkoski, Ujjwol Tamrakar, Nikos Hatziargyriou, and Dimitris. 2019. Microgrid stability definitions, analysis, and examples. *IEEE Transactions on Power Systems Lagos* 35(1):13-29.

Firdaus, Ayesha, and Sukumar Mishra. 2019. Mitigation of power and frequency instability to improve load sharing among distributed inverters in microgrid systems. *IEEE Systems Journal* 14 (1):1024-1033.

Gajbhiye, Shraddha, and Navita Khatri. 2021. Modified Robust Droop Control Based On Arctan Control Strategy For Proportional Load Sharing Between Parallel Operated Inverters. 2021 IEEE Transportation Electrification Conference (ITEC-India).

Gupta, Tripti, and D. K. Sambariya. 2017. Optimal design of fuzzy logic controller for automatic voltage regulator. 2017 International Conference on Information, Communication, Instrumentation and Control (ICICIC).

Harun, Li Yang, and Irina. 2022. Renewable energy scenarios for sustainable electricity in Malaysia and the application of analytical hierarchy process (AHP) for decision-making. *J. Kejuruter.* 34:1271-1279.

Huang, Xuezheng, and Changsong Chen. 2020. Improved Droop Control Scheme for Reactive Power Sharing of Parallel Inverter System. 2020 IEEE 1st China International Youth Conference on Electrical Engineering (CIYCEE).

Jia, Yaoqin, Junjie Xiao, Biao Jia, Yujian Pan, Yunpeng Wang, and Zhifan Li. 2020. Improved droop control based on multi-stage lead-lag compensation. IECON 2020 The 46th Annual Conference of the IEEE Industrial Electronics Society.

John, Blessy, Arindam Ghosh, and Firuz Zare. 2017. Load sharing in medium voltage islanded microgrids with advanced angle droop control. *IEEE Transactions on Smart Grid* 9 (6):6461-6469.

Khaledian, Amir, and Masoud Aliakbar Golkar. 2017. Analysis of droop control method in an autonomous microgrid. *Journal of Applied Research and Technology* 15 (4):371-377.

Kim, Jaehong, Josep M Guerrero, Pedro Rodriguez, Remus Teodorescu, and Kwanghee Nam. 2010. Mode adaptive droop control with virtual output impedances for an inverter-based flexible AC microgrid. *IEEE Transactions on Power Electronics* 26 (3):689-701.

Kljajić, Ružica, Predrag Marić, Hrvoje Glavaš, and Matej Žnidarec. 2020. Microgrid Stability: A Review on Voltage and Frequency Stability. 2020 IEEE 3rd International Conference and Workshop in Óbuda on Electrical and Power Engineering (CANDO-EPE).

Kolluri, Ramachandra Rao, Iven Mareels, Tansu Alpcan, Marcus Brazil, Julian de Hoog, and Doreen Anne Thomas. 2017. Power sharing in angle droop controlled microgrids. *IEEE Transactions on Power Systems* 32(6):4743-4751.

Kulkarni, Shreeram V, and Dattatraya, N. 2021. "Improved droop control strategy for parallel connected power electronic converter based distributed generation sources in an Islanded Microgrid. *J. Electric Power Systems Research Gaonkar* 201: 107531.

Li, Zilin, Ka Wing Chan, Jiefeng Hu, and Josep, M. 2020. Adaptive droop control using adaptive virtual impedance for microgrids with variable PV outputs and load demands. *J. IEEE Transactions on Industrial Electronics Guerrero* 68(10): 9630-9640.

Liu, Shuai, Li Wei, and Huai, Wang. 2020. Review on reliability of supercapacitors in energy storage applications. *J Applied Energy* 278: 115436.

Mahdavian, Aram, Ali Asghar Ghadimi, and Mohammad Bayat. 2021. Microgrid small-signal stability analysis considering dynamic load model. *J IET Renewable Power Generation* 15(13): 2799-2813.

Matharani, K., and H. Jariwala. 2023. Stability Analysis of Microgrid with Passive, Active, and Dynamic Load. *Journal of Operation and Automation in Power Engineering* 11(4): 295-306. doi: 10.22098/joape.2024.10445.1741.

Moussa, Hassan, Ahmed Shahin, Jean-Philippe Martin, Serge Pierfederici, and Nazih Moubayed. 2017. Optimal angle droop for power sharing enhancement with stability improvement in islanded microgrids. *IEEE Transactions on Smart Grid* 9(5): 5014-5026.

Pogaku, Nagaraju, Milan Prodanovic, and Timothy C Green. 2007. Modeling, analysis and testing of autonomous operation of an inverter-based microgrid. *IEEE Transactions on Power Electronics* 22 (2):613-625.

Praiselin, W. J. & J. Belwin. 2022. Enhancement of power-sharing using multivariable angle droop control for inverter interfaced distributed generations in a micro-grid. *Journal of Electrical Engineering Edward, and Technology* 17(6): 3155-3167.

Rahmani-Andebili, Mehdi. 2021. *Applications of Fuzzy Logic in Planning and Operation of Smart Grids*: Springer.

Raju, PESN, and Trapti Jain. 2019. "Development and validation of a generalized modeling approach for islanded inverter-based microgrids with static and dynamic loads." *International Journal of Electrical Power & Energy Systems* 108:177-190.

Rasheduzzaman, Md, Jacob A Mueller, and Jonathan W Kimball. 2014. An accurate small-signal model of inverter-dominated islanded microgrids using dq reference frame. *IEEE Journal of Emerging and Selected Topics in Power Electronics* 2(4):1070-1080.

Shahgholian, Ghazanfar International Transactions on Electrical Energy Systems. 2021. A brief review on microgrids: Operation, applications, modeling, and control. 31 (6):e12885.

Shi, Yuntao, Xiang Gu, Xiang Yin, Shun Feng, and Shufeng Zhang. 2022. Design of droop controller in islanded microgrids using multi-objective optimisation based on accurate small-signal model. *IET Power Electronics* 15(11): 1093-1109.

Shuai, Zhikang, Wen Huang, Xia Shen, Yifeng Li, Xin Zhang, and Z. John Shen. 2018. A maximum power loading factor (MPLF) control strategy for distributed secondary frequency regulation of islanded microgrid. *J IEEE Transactions on Power Electronics* 34 (3): 2275-2291.

Song, Yong-Hua, and Allan T. Johns. 1997. Applications of fuzzy logic in power systems. Part 1: General introduction to fuzzy logic. *J Power Engineering Journal* 11(5): 219-222.

Yamashita, Daniela Yassuda, Ionel Vechiu & Jean-Paul Gaubert. 2020. A review of hierarchical control for building microgrids. *Sustainable Energy Reviews* 118: 109523.

Yu, Kai, Qian Ai, Shiyi Wang, Jianmo Ni, and Tianguang Lv. 2015. Analysis and optimization of droop controller for microgrid system based on small-signal dynamic model. *IEEE Transactions on Smart Grid* 7 (2):695-705.

Zafari, Pegah, Ali Zangeneh, Mohammad Moradzadeh, Alireza Ghafouri & Moein Aldin Parazdeh. 2020. Various droop control strategies in microgrids. *Microgrid Architectures Control, and Protection Methods:* 527-554.

Zhang, Liang, Hao Zhen, Quangui Hu, Bin Su, and Ling IEEE Access Lyu. 2019. An adaptive droop control strategy for islanded microgrid based on improved particle swarm optimization 8: 3579-3593.